Research Square

Preprints are preliminary reports that have not undergone peer review.
They should not be considered conclusive, used to inform clinical practice,
or referenced by the media as validated information.

Optimization of Cold-Start Strategies for Seawater Pumps in Polar Ice Conditions

Fukang Ma
North University of China
Yuxiang Chen
North University of China
Chiyu Wang
North University of China
Lingfei Kong
North University of China
Zhengyang Liu
North University of China
Kai Zhang
North University of China
Ruifan Xu
ruifanxu@mail.ustc.edu.cn

University of Science and Technology of China

Article

Keywords: Polar ice conditions, seawater pumps, cold start, ice crystals, multiphase flow

Posted Date: March 3rd, 2026

DOI: https://doi.org/10.21203/rs.3.rs-8860812/v1

License: This work is licensed under a Creative Commons Attribution 4.0 International License.
Read Full License

Additional Declarations: No competing interests reported.

Type of the Paper (Article)

Optimization of Cold-Start Strategies for Seawater Pumps in Polar Ice Conditions

Fukang Ma[1],Yuxiang Chen[1], Chiyu Wang[1], Lingfei Kong[1],Zhengyang Liu[1], Kai Zhang[1], Ruifan Xu[2*]

1 School of Energy and Power Engineering, North University of China, Taiyuan , Shanxi 030051, China
2 State Key Laboratory of Fire Science, University of Science and Technology of China, Hefei 230027, Anhui, China
*Corresponding author: Ruifan Xu
*the Email Address of the Corresponding Author: ruifanxu@mail.ustc.edu.cn.

Abstract: Seawater pumps operating in polar low-temperature, ice-laden environments are subject to a high risk of start-up failure, in which the transport, accumulation, and blockage of ice crystals within the pump play a critical role in determining start-up reliability. To investigate the cold-start behavior of seawater pumps under polar ice conditions, a transient multiphase numerical model incorporating ice–water two-phase coupling effects is developed. The model is employed to systematically examine the influences of the motor acceleration index and the impeller–volute clearance on ice-crystal blockage risk and start-up response characteristics.For a representative operating condition with an ice-crystal volume fraction of 10%, the transient internal flow and phase distribution evolution are simulated using an Eulerian–Eulerian multiphase framework, and the numerical predictions are validated against experimental results. The results demonstrate that the acceleration index primarily affects the start-up stabilization time and peak torque by regulating the rotational speed ramp-up rate and the unsteady evolution of the flow field during the start-up process; however, its contribution to improving ice-crystal passability is relatively indirect. In contrast, the impeller clearance significantly reshapes ice-crystal transport pathways by modifying leakage-flow intensity and flow connectivity, thereby providing a more direct and sustained mitigation of localized high-concentration accumulation and blockage risks. These findings offer quantitative guidance for the optimization of start-up strategies and the design of anti-blockage structures for seawater pumps operating in polar regions.

Keywords: Polar ice conditions; seawater pumps; cold start; ice crystals; multiphase flow

1. Introduction

With the rapid advancement of polar shipping, polar marine engineering equipment, and resource exploitation activities in high-latitude regions, increasing attention has been directed toward the operational safety and reliability of seawater pumps, which serve as critical power and cooling components, under low-temperature and ice-laden conditions[1][2]. In polar seas, the combined effects of seawater supercooling and turbulent disturbances promote the formation of fine ice crystals, commonly referred to as frazil ice, which exist in suspension or flocculated forms within the water column. These ice crystals can be entrained into the pump with the incoming flow and subsequently accumulate and deposit in the impeller passages, flow channels, and narrow clearance regions, leading to severe operational issues such as flow passage blockage, flow-rate degradation, and even pump failure[3-5].

Extensive studies have been conducted on the generation and evolution mechanisms of ice crystals, in which the formation conditions, particle-size distribution characteristics, and transport behavior under varying salinity levels and turbulence intensities have been systematically analyzed

from thermodynamic and hydrodynamic perspectives [6-8]. Experimental investigations have demonstrated that ice crystals in seawater are prone to flocculation, forming larger ice agglomerates whose dynamic behavior differs substantially from that of conventional solid particles [9]. In the context of hydraulic structures and seawater intake systems, further studies have identified ice-crystal aggregation and bridging as primary mechanisms responsible for freezing and blockage in intake facilities [10-12].

By contrast, existing studies on seawater pumps operating in low-temperature or polar environments have primarily focused on material property degradation, variations in lubrication characteristics, and transient hydraulic responses during the start-up process [13-15]. In most of these investigations, the working medium is assumed to be a single-phase liquid, and the presence of ice crystals is neglected, which limits the applicability of the reported conclusions to ice-laden operating conditions in polar regions. Meanwhile, although research on seawater pumps handling solid–liquid two-phase flows has become relatively mature, the solid phase is typically represented by sand particles or other rigid materials. Such models fail to adequately capture the deformability, adhesiveness, and phase-change characteristics exhibited by ice crystals under low-temperature conditions [16][17].

During the start-up stage, the internal flow within a seawater pump has not yet developed a stable structure, and the rotational speed, pressure, and flow rate exhibit pronounced unsteady characteristics. This stage is therefore considered a high-risk period for the ingress and accumulation of ice crystals within the pump [13][18]. Previous studies have demonstrated that the start-up mode plays a crucial role in the evolution of the transient internal flow field, with the start-up acceleration rate directly governing the speed ramp-up process and, consequently, influencing the intensity of unsteady flow fluctuations and the formation of internal recirculation structures [14][15]. However, the mechanisms by which start-up acceleration affects ice-crystal passability and blockage risk remain poorly understood and lack systematic investigation.On the other hand, the impeller clearance, as a key structural parameter of seawater pumps, has been shown through numerous numerical and experimental studies to significantly affect leakage flow, recirculation patterns, and hydraulic efficiency [19-21]. Variations in clearance size have been reported to substantially alter flow connectivity and the distribution of low-velocity stagnant regions. Nevertheless, existing studies have yet to explicitly link impeller clearance with ice-crystal transport behavior. Under low-temperature, ice-laden operating conditions, the potential influence of impeller clearance on ice-crystal transport pathways, accumulation locations, and blockage formation remains insufficiently explored and warrants further investigation.

In addition, seawater temperature, as a key physical boundary condition in polar environments, not only affects fluid viscosity and flow resistance but also directly governs the generation state and stability of ice crystals, thereby exerting a fundamental control over ice-crystal behavior during the cold-start process. Although extensive studies have examined ice-crystal formation mechanisms, intake blockage phenomena, and the performance of seawater pumps under solid–liquid two-phase flow conditions, few efforts have systematically compared the coupled effects of start-up control parameters, particularly the acceleration index, and the impeller–volute clearance on ice-crystal passability, head development, and peak load during cold start-up under low-temperature, ice-laden conditions.

Based on the above analysis, this study conducts a systematic numerical investigation of the cold-start process of seawater pumps operating under low-temperature, ice-laden conditions. The main contributions of this work are summarized as follows: (1) a transient numerical model for the cold start-up of a seawater pump is developed with explicit consideration of ice-crystal transport characteristics, enabling the dynamic evolution of pump head and shaft power under ice-laden conditions to be captured; (2) from the perspective of start-up control parameters, the influence mechanisms of the acceleration rate on ice-crystal retention, head build-up, and peak torque are systematically analyzed for the first time; (3) the regulatory role of the impeller–volute clearance on internal flow structures and ice-crystal passability during ice-laden start-up is further elucidated, and

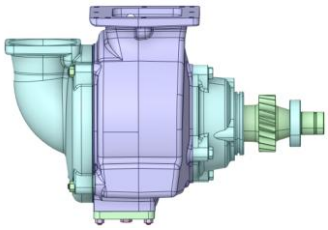
corresponding engineering implications are provided. The present study offers quantitative guidance for the optimization of start-up strategies and the design of anti-blockage structures for seawater pumps operating in polar environments.

2. Methodology

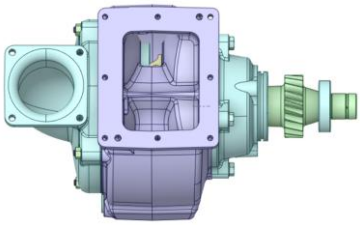
2.1. Geometry and Computational Domain

In this study, a single-stage seawater pump employed in practical engineering applications is selected as the research object (as shown in Figure 1, with geometric parameters listed in Table 1). The pump is widely used in cooling and transport systems of marine engineering equipment, and its structural configuration and operating conditions are representative of similar seawater pumps in engineering practice. As such, it is capable of capturing the typical hydraulic response characteristics of seawater pumps during the cold-start process under low-temperature, ice-laden polar environments. To systematically investigate the transient flow evolution and ice-crystal transport behavior during the cold-start stage, a complete three-dimensional geometric model is established based on the actual pump configuration.

The computational domain consists of key hydraulic components, including the impeller, the volute, and the impeller – volute clearance. The impeller region serves as the core zone for energy input and momentum transfer during start-up, directly governing the speed ramp-up process and the evolution of the primary internal flow field. The volute and tongue regions are responsible for the conversion of kinetic energy into pressure energy and constitute critical locations where recirculation structures and low-velocity stagnant zones tend to form during start-up, making them closely associated with the local retention and accumulation of ice crystals. The impeller – volute clearance, as an important structural parameter of the pump, significantly affects leakage-flow intensity and flow connectivity between high- and low-pressure regions, thereby exerting a pronounced influence on ice-crystal transport pathways and distribution characteristics under ice-laden conditions. Given that this study focuses on elucidating the role of clearance on cold-start performance and ice-crystal passability, the impeller – volute clearance is parameterized in the numerical model to enable comparative analyses among different clearance configurations while maintaining all other structural parameters unchanged.



(a) Seawater pump front view



(b) Top view of seawater pump

Figure1 Seawater pump solid model

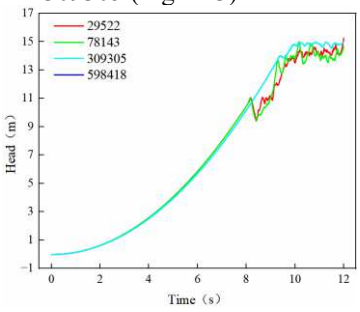
Table 1 Centrifugal pump main geometric parameters

Structure name	Parameters
Design Flow Rate (m^3 /h)	65

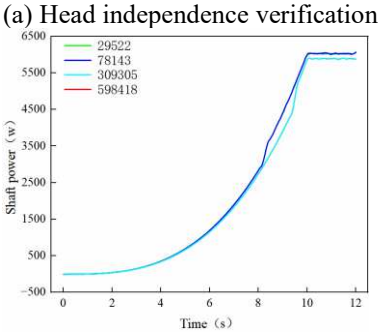
Design Head (m)	15
Design Speed (r/min)	1800
Start-up Time (s)	10
Shaft Power (kW)	6
Inlet/Outlet Pressure Difference (MPa)	0.12
Number of Impeller Blades	3

2.2. Mesh and Irrelevantity

In the geometric modeling process, to balance computational efficiency and physical reliability, local structural details with minimal impact on cold start transient flow and ice crystal transport were appropriately simplified without altering the shape of the main flow channel and critical gap structure within the pump. SpaceClaim was used to mesh the fluid domain, with local mesh refinement near the impeller. Simulations were performed using mesh numbers 29522, 78143, 309305, and 598418. Mesh independence was verified using head and shaft power, as shown in Figure 2. The computational differences were small. To save computational resources and time, mesh number 309305 (Figure 3) was selected for subsequent calculations.



(a) Head independence verification



(b) Shaft power independence verification

Figure2 Mesh independence verification

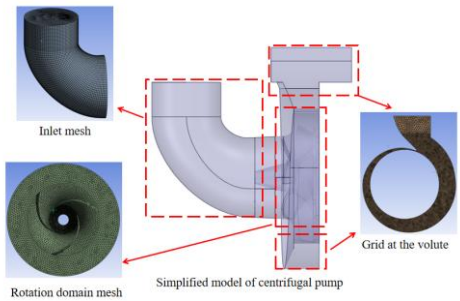


Figure3 Model Mesh

2.3. Governing equations and turbulence models

The continuity equation in fluid mechanics is a mathematical expression used to describe the conservation of mass during fluid flow. It is one of the fundamental equations of fluid mechanics, ensuring that mass neither arises nor disappears during fluid flow, and that the total mass of the fluid remains constant. Specifically, it means that the increase in the mass of fluid in a small element per unit time is equal to the net mass flowing into that small element during the same time interval. Based on this law, the mass conservation equation, i.e., the continuity equation, can be derived:

$$\frac{\partial \rho}{\partial t} + \nabla \bullet (\rho v) = 0 \quad (1)$$

Fluids not only satisfy the conservation of mass but also the conservation of momentum, based on Newton's second law. Since in fluid mechanics, fluid is a continuous medium, its momentum constantly changes with time and space. Therefore, we need to distribute force, mass, and acceleration into every tiny volume of the fluid, that is, a micro-element body. In computational fluid dynamics, it is expressed as: the change rate of the momentum of the fluid in the micro-element body with respect to time is equal to the resultant external force acting on the micro-element body. According to this law, the momentum equation can be derived as follows:

$$\rho \frac{\partial v}{\partial t} + \rho(v \bullet \nabla)v = -\nabla p + \mu \nabla^2 v + \rho g \quad (2)$$

Flow problems also obey the law of conservation of energy. Based on this law, we can conclude that the total energy change within a control volume equals the net input of heat and work through the boundary. The energy equation is the mathematical expression of the law of conservation of energy, revealing the interaction of internal energy, kinetic energy, and thermal energy in a fluid. It combines the effects of convection, conduction, viscous dissipation, and external sources, and can be expressed as:

$$\frac{\partial (\rho E)}{\partial t} + \nabla \cdot (\rho E U) = -\nabla \cdot (q) + \nabla \cdot (\tau \cdot u) + \rho S_E \quad (3)$$

It is generally believed that the unsteady continuity equation and the Navier-Stokes equation are applicable to all transient turbulent motions. Through comparative analysis of turbulence models, the RNG k-ε model has the least impact on computational accuracy in this simulation. Therefore, this paper uses the RNG k-ε turbulence model to simulate the turbulent field. The governing equations for turbulent kinetic energy k and dissipation rate ε are as follows:

$$\frac{\partial (\rho k)}{\partial t} + \frac{\partial (\rho k u_i)}{\partial x_i} = \frac{\partial}{\partial x_i}\left(\alpha_k \mu_{eff} \frac{\partial k}{\partial x_i}\right) + G_k - \rho \varepsilon \quad (4)$$

$$\frac{\partial (\rho \varepsilon)}{\partial t} + \frac{\partial \left(\rho u_j \varepsilon\right)}{\partial x_{\mathrm{j}}} = \frac{\partial}{\partial x_{\mathrm{j}}}\left[\left(\mu + \frac{\mu_t}{\sigma_\varepsilon}\right)\frac{\partial \varepsilon}{\partial x_j}\right] + C_{1\varepsilon}\frac{\varepsilon}{k}G_k - C_{2\varepsilon}\rho\varepsilon^2\frac{1}{k}R_\varepsilon \quad (5)$$

Where ρ denotes the fluid density; t is time; v is the fluid velocity vector; $\nabla(\rho v)$ represents the spatial variation of the mass flux; $-\nabla p$ is the pressure gradient; $\mu \nabla^2 v$ denotes the viscous force term; ρg is the body force per unit volume; E is the total energy; u is the velocity vector; q is the heat flux vector; τ is the viscous stress tensor; S_E represents an external heat source; μ_t is the turbulent viscosity; G_k denotes the production term of turbulent kinetic energy; σ_ε is the turbulent Prandtl number for ε; $C_{1\varepsilon}$ and $C_{2\varepsilon}$ are model constants of the turbulence model; and R_ε is the additional correction term introduced in the RNG formulation.

2.4. Selection of multiphase flow model

Under low-temperature, ice-laden cold-start conditions in polar environments, the internal flow within a seawater pump constitutes a typical multiphase flow problem, the physical characteristics of which are jointly governed by the ice-crystal volume fraction, particle size, and the intensity of interphase interactions. For different ice-laden conditions, the appropriate selection of a multiphase flow model is therefore critical to ensuring the reliability of numerical simulations.

The Volume of Fluid (VOF) model tracks distinct phase interfaces through volume-fraction transport equations and is well suited for problems involving free surfaces or continuous phase interfaces. However, ice crystals formed during the cold-start process generally exist as dispersed particles rather than forming stable, trackable continuous interfaces. Consequently, the VOF model

is not well suited to accurately describing ice-crystal transport and accumulation, particularly at high volume fractions, where non-physical interface diffusion may occur.

When the ice-crystal volume fraction is relatively low (typically below 1%), the Discrete Phase Model (DPM) can be employed to track individual ice crystals in a Lagrangian framework, enabling detailed analysis of particle trajectories, residence time, and localized retention behavior. As the volume fraction increases, however, the number of particles rises sharply, leading to prohibitive computational costs and reduced applicability of the DPM, while collective effects arising from particle – particle and particle – fluid interactions become increasingly difficult to capture.

For representative polar operating conditions with an ice-crystal volume fraction of approximately 10%, ice crystals exhibit quasi-continuous phase behavior, and their momentum feedback on the carrier flow can no longer be neglected. Under such circumstances, continuum-based Eulerian – Eulerian or Mixture models provide a more appropriate framework for describing the two-way coupling between the ice and water phases. Among these approaches, the Eulerian – Eulerian model solves separate mass and momentum conservation equations for each phase, enabling accurate representation of the spatial evolution and local accumulation of high-concentration ice crystals within the pump. This model is particularly suitable for analyzing operating conditions prone to particle accumulation or bridging.

Based on the above considerations, the Eulerian – Eulerian multiphase flow model is adopted in this study to simulate the transient ice-laden flow within the pump during cold start-up at an ice-crystal volume fraction of 10%, thereby ensuring a physically consistent description of ice-crystal transport, accumulation, and their influence on the internal flow field.

Under the assumption that phase-change processes such as melting and freezing of ice crystals are neglected, no mass transfer occurs between the ice and water phases. Accordingly, the volume fraction of the ice phase satisfies the following transport equation:

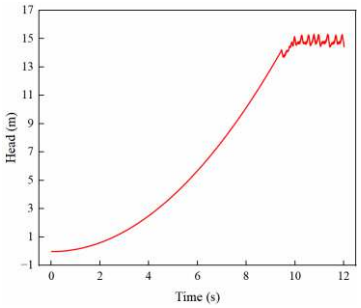
$$\frac{\partial \alpha_i}{\partial t} + \nabla \cdot (\alpha_i u_i) = 0 \tag{6}$$

Where α_i denotes the volume fraction of the ice phase, ranging from 0 to 1, and u_i represents the phase-averaged velocity of the ice phase.

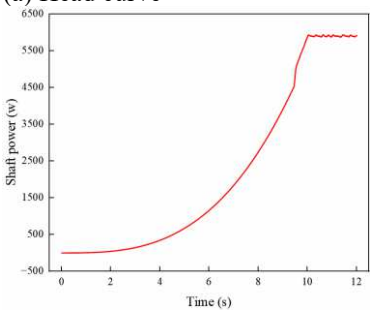
2.5. Boundary condition setting and experimental verification

To investigate the cold-start behavior of the seawater pump, a velocity-inlet boundary condition is imposed at the pump inlet, with the inlet velocity prescribed as 2.5 t/10, reaching a maximum value of 2.5 m/s at t=10s. A pressure-outlet boundary condition is applied at the pump outlet. The impeller is defined as a rotating domain, while all other components are treated as stationary domains.

As shown in Figure 4, the numerical predictions at the stabilized stage of start-up are compared with experimental measurements of an actual seawater pump under cold-start conditions in terms of pump head, shaft power, and inlet–outlet pressure difference. The experimentally measured head, shaft power, and pressure difference obtained from low-temperature tests are summarized in Table 1, while the corresponding numerical results are illustrated in Figure 4. At the stabilized start-up stage, the predicted pump head fluctuates around 15 m, and the shaft power remains approximately 0.58 MPa. The relative deviation between numerical and experimental results is on the order of 0.03%, with the overall error remaining within 5%. These results indicate that the developed numerical model exhibits satisfactory accuracy and is suitable for subsequent analyses, including lubrication system investigations.



(a) Head curve



(b) Shaft power curve

Figure4 Simulation result diagram

3. Results and discussion

3.1 The effect of ice content on startup performance

Before entering the seawater pump, the inflowing seawater passes through a filter screen. Considering that the maximum ice-crystal particle size allowed to pass through the upstream filter of the investigated pump is 1 mm, a uniform ice-crystal diameter of 1 mm is adopted in this study, with a corresponding volume fraction of 10%.

Figures 5 and 6 compare the variations in pump head and shaft power during the cold-start process under pure seawater and ice-laden operating conditions. Under ice-laden conditions, the effective viscosity and apparent density of the mixture are altered, while the presence of ice crystals introduces additional local resistance and particle–blade interactions. As a result, the ability of the impeller to perform work on the fluid is reduced, leading to a decrease in pump head during the start-up stage. Meanwhile, the shaft power demand increases. These results indicate that even at a moderate ice-crystal volume fraction, the ice phase exerts a non-negligible influence on the cold-start hydraulic response and the associated driving load of the seawater pump.

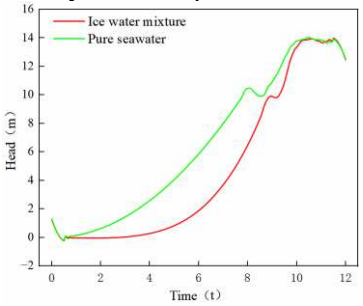


Figure5 The impact of ice crystals on head during startup

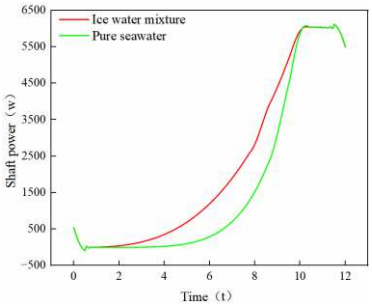


Figure6 The effect of ice crystals on shaft power during startup

3.2. Study on the effect of variable acceleration on ice crystal blockage and start-up response

Under polar low-temperature, ice-laden conditions, the speed ramp-up process during the cold start of a seawater pump governs the development of transient pressure gradients, recirculation structures, and the interphase transport environment within the pump. These factors jointly influence head build-up, peak load demand, and the short-term accumulation risk of ice crystals in critical regions. To characterize different start-up strategies, an exponential speed ramp function is adopted in this study, expressed as $n(t) = n_0 \left(\frac{t}{t_s}\right)^k$,where k denotes the acceleration index and t_s is the prescribed start-up duration. Comparative analyses are performed under ice-laden conditions with an ice-crystal volume fraction of 10% and a particle diameter of 1 mm to assess the influence of different acceleration indices on start-up response and ice-related risks.

(1) Start-up stabilization time and head convergence

To avoid subjective bias in determining the stabilization time, the start-up stabilization time t_{st} is defined as the earliest time at which the head curve $H(t)$ first enters and remains within ±2% of the steady-state mean head H_{ss} for no less than 0.5 s. Based on this criterion, t_{st} values corresponding to different acceleration indices are extracted from Figure8, with the results summarized in Table 2.

Overall, variations in the acceleration index affect head convergence by altering the speed ramp-up rate and the characteristic time scale of flow-field reorganization. A larger acceleration index results in a smoother speed increase, leading to slower establishment of the main flow kinetic energy and a prolonged head rise and convergence process, thereby delaying satisfaction of the stabilization criterion. In contrast, a smaller acceleration index enables more rapid speed establishment and earlier entry of the head into the steady-state range, but is often accompanied by stronger transient fluctuations. This behavior reflects a competing effect between faster convergence and increased unsteady oscillations during start-up.

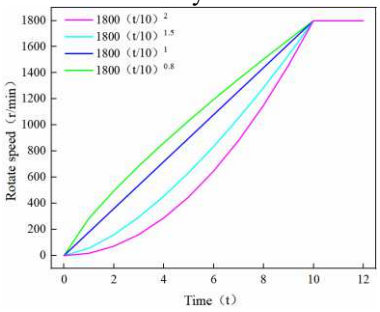


Figure7 Time-speed graph

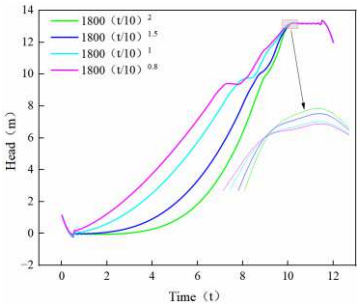


Figure8 Time-lift chart

Table 2 Steady-state head and settling time

Acceleration exponent k	steady-state average head H_{ss} (m)	±2% interval	earliest time t (s) to meet steady-state criterion
2	13.3	13.03 – 13.56	9.6
1.5	13.2	12.94 – 13.46	9.3
1	13.1	12.84 – 13.36	9
0.8	13	12.74 – 13.26	8.6

(2) Peak start-up torque

The peak start-up torque represents the maximum load that must be overcome by the pump during the start-up process. The acceleration index directly affects the motor output power and consequently determines the torque demand. Based on the shaft power and rotational speed data, The peak torque during startup can be calculated using the following formula:

$$T_{max} = \frac{P_{max} * 60}{2\pi n} \quad (7)$$

As shown in Figure 9, the peak start-up torque exhibits an increasing trend as the acceleration index decreases. When the acceleration index is reduced to k=0.8, the peak torque reaches 32.1 N· m at a rotational speed of 1800 r/min, whereas a higher acceleration index of k=2 results in a lower peak torque of 30.8 N· m under the same speed condition. These results indicate that more aggressive speed ramp-up strategies impose higher torque demands during start-up, which may place greater constraints on the driving system.

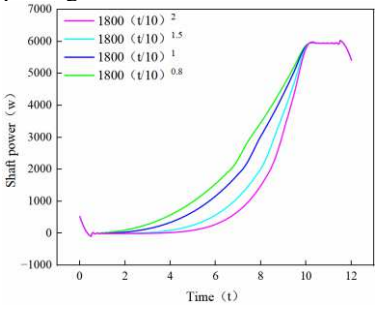


Figure9 Time-axis power graph

Table 3 Peak torque and corresponding time

Acceleration exponent k	Peak power P_{max} (W)	Corresponding time t (s)	Rotational speed n (r/min)	Peak torque T_{max} （N • m）
2	5800	11.0	1800	30.8
1.5	5900	10.8	1800	31.3
1	6000	10.5	1800	31.8

0.8	6050	10.0	1800	32.1

(3) Start-up energy consumption

The start-up energy consumption E_{start} is defined as the total energy consumed by the pump from the onset of start-up until stable operation is achieved. It is obtained by integrating the shaft power over time as:

$$E_{start} = \int_0^{t_s} P(t)dt \quad (8)$$

where the upper integration limit t_{st} corresponds to the stabilization time defined previously, representing the energetic cost required to reach stable operation.Figure 9 shows the E_{start} values for each operating condition.

From a mechanistic perspective, start-up energy consumption is governed jointly by the average power level and the effective duration of the start-up process. As summarized in Table 4, decreasing the acceleration index shortens the stabilization time and thus reduces the integration interval, leading to a decrease in start-up energy consumption in the present cases. Meanwhile, faster speed ramp-up tends to increase instantaneous power peaks. The combined effect of these two competing factors ultimately determines the overall energy expenditure during start-up.

Table 4 Startup energy consumption and startup time

Acceleration exponent k	Startup time t (s)	Startup energy consumption E (kJ)	Relative level
0	9.8	31	Maximum
2	9.5	29.8	Relatively high
5	9.2	28.5	Moderate
8	9	27.8	Minimum

(4) Flow structure evolution and ice-crystal transport risk

Although velocity contour plots cannot directly quantify the ice-crystal passing rate, they are effective in identifying flow features closely associated with blockage risk, such as low-velocity stagnant zones, closed recirculation structures, and variations in main-flow channel connectivity. These features provide a flow-structure-based interpretation of ice-crystal accumulation tendencies. As shown in Figure 10, under larger acceleration indices, the rotational speed builds up more slowly during the early startup stage, and the main flow kinetic energy and pressure difference inside the pump are insufficiently established. As a result, pronounced low-velocity stagnant regions persist near the impeller inlet and along the volute wall, accompanied by weak recirculation structures. Once ice crystals enter these regions, their convective transport capability is significantly reduced, making their trajectories more prone to deviation from the main flow path and short-term retention. This behavior increases both the local accumulation probability and residence time in critical regions, thereby leading to a higher blockage risk.

With decreasing acceleration index, the impeller speed is established within a shorter time, resulting in an overall increase in the internal flow velocity level. The velocity field becomes more continuous, while the spatial extent of low-velocity zones and recirculation structures is markedly reduced, and the connectivity of the main flow channel is enhanced. The strengthened main-flow transport capacity facilitates the rapid discharge of ice crystals along the primary flow path, reducing their residence probability in sensitive regions such as the inlet and near-wall areas, which is beneficial for improving the passing stability during ice-laden cold startup conditions.

When the acceleration index is further reduced to relatively low levels, although the main-flow transport capacity continues to increase, the non-stationary characteristics during the early startup stage are simultaneously intensified. Local velocity and pressure gradients become more pronounced, manifested by enhanced transient entrainment, strengthened vortex structures, and increased local velocity fluctuations. Under such conditions, the dispersion of ice-crystal trajectories

may increase, leading to diminishing marginal benefits from the contraction of low-velocity regions. In other words, while ice crystals are more readily discharged, their transient trajectory fluctuations and localized aggregation–dispersion behavior may also be enhanced. Overall, the startup acceleration index indirectly affects ice-related blockage risk by modifying low-velocity and recirculation structures and reshaping particle transport pathways. Its mitigation effect tends to saturate at higher acceleration levels and therefore must be jointly balanced with peak torque constraints to determine an optimal startup strategy.

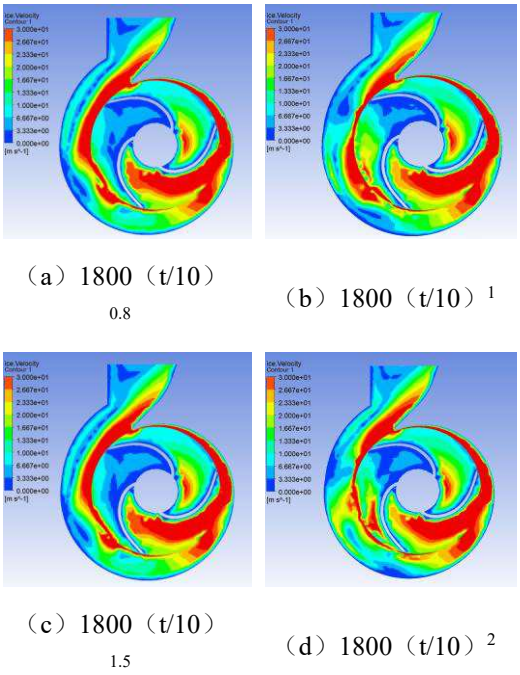


Figure10 Seawater pump velocity cloud map

3.3. Research on the effect of impeller clearance on ice crystal blockage and start-up response

The impeller–volute clearance modifies the intensity of internal leakage flow and the connectivity between high- and low-pressure regions, thereby reshaping the transient flow-field topology and ice-crystal transport pathways during the startup stage at a structural level. In contrast to the acceleration profile, which primarily affects flow establishment through temporal scaling, the clearance parameter directly alters spatial flow channels. As a result, it exhibits a more persistent structural significance in controlling ice-related startup risks. In this study, different clearance configurations were realized by adjusting the impeller diameter relative to an initial reference clearance, and their effects on startup response and ice-laden risk characteristics were systematically compared.

(1) Start-up stabilization time and head convergence

The startup stabilization time t_s was determined using the same criterion as defined in Section 3.2, and the corresponding values under different clearance conditions were extracted from Figure 11 and summarized in Table 5. The results indicate that increasing the clearance generally accelerates the head buildup process during startup while reducing fluctuation intensity, leading to an overall shortening of the stabilization time. This behavior suggests that moderate clearance-induced leakage flow can partially “open up” internal flow connections during the early startup stage, enabling faster flow-field reorganization and earlier attainment of a quasi-steady state. It should be noted, however, that excessive clearance may introduce volumetric losses and degrade steady-state efficiency. Therefore, a trade-off between startup reliability and steady-state performance is required.

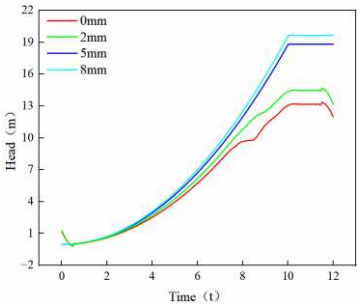


Figure11 Time-lift chart

Table 5 Steady-state head and settling time

Gap (mm)	steady-state average head H_{ss} (m)	±2% interval	earliest time t (s) to meet steady-state criterion
0	13.2	12.94–13.46	9.8
2	14	13.72–14.28	9.5
5	18.8	18.42–19.18	9.2
8	19.5	19.11–19.89	9

(2) Peak start-up torque

The peak startup torque was calculated following the same method as in Section 3.2, and its variation with clearance is shown in Figure 12 and Table 6. As the clearance increases, the peak torque demand during startup exhibits a clear decreasing trend. Physically, a larger clearance provides an additional leakage return path for high-pressure fluid, which weakens the instantaneous pressure differential and hydrodynamic resistance that must be established by the impeller during startup. Consequently, the peak torque requirement imposed on the motor is reduced. Under low-temperature operating conditions, this effect is particularly beneficial, as it alleviates startup shock loads and enhances mechanical and driving reliability.

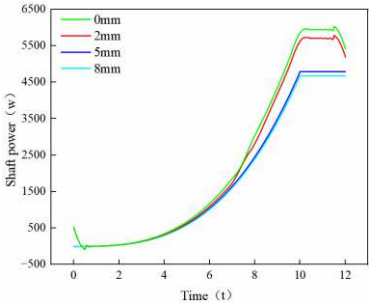


Figure12 Time-axis power graph

Table 6 Peak torque and corresponding time

Gap (mm)	Peak power P_{max} (W)	Corresponding time t (s)	Rotational speed n (r/min)	Peak torque T_{max} （N·m）
0	6000	10	1800	31.8
2	5800	10	1800	30.8
5	4800	10.2	1800	25.5
8	4700	10.2	1800	24.9

(3) Start-up energy consumption

The startup energy consumption was also evaluated following the procedure described in Section 3.2. With increasing clearance, both the peak power level and the stabilization time tend to decrease, resulting in a monotonic reduction in the total startup energy E_{start}, as summarized in Table 7. This behavior differs from that observed for variations in the acceleration index: clearance enlargement improves startup responsiveness without significantly increasing instantaneous power peaks, highlighting its combined advantages in controlling both energy consumption and mechanical load during cold startup conditions.

Table 4 Startup energy consumption and startup time

Gap (mm)	Startup time t (s)	Startup energy consumption E (kJ)	Relative level
0	9.8	31	Maximum
2	9.5	29.8	Relatively high
5	9.2	28.5	Moderate
8	9	27.8	Minimum

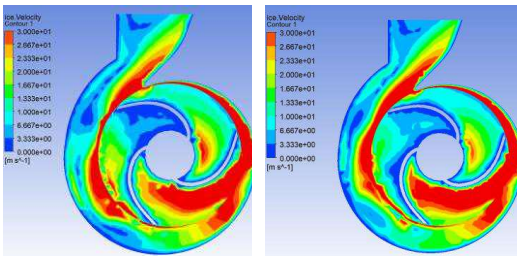
(4) Flow structure evolution and ice-crystal transport risk

The ice-crystal passing behavior, inferred from Figure 13, reveals that clearance variation exerts a more direct influence on the velocity field than acceleration-based strategies. Its dominant effects are reflected in three aspects: (1) modification of leakage and recirculation channel strength, (2) changes in the spatial location and scale of low-velocity stagnant zones and closed recirculation structures, and (3) enhancement or degradation of main-flow channel connectivity. Together, these factors determine whether ice crystals are prone to short-term accumulation in critical regions such as the impeller inlet, near-wall areas, and the volute tongue, potentially evolving into bridging and blockage risks.

When the clearance is small, leakage paths between high- and low-pressure regions are restricted, and the startup flow tends to exhibit a “localized high-pressure-difference–strong separation” pattern. Under such conditions, low-velocity stagnant zones readily form near the impeller inlet and blade passages close to the wall, while closed recirculation or secondary flow entrainment is more likely to develop near the volute tongue. These flow structures are unfavorable for ice-laden transport: ice crystals entering low-velocity regions experience insufficient convective carrying capacity and tend to stagnate, whereas closed recirculation causes repeated particle circulation and short-term accumulation, thereby increasing the likelihood of ice bridging and blockage.

With a moderate increase in clearance, velocity contours indicate enhanced leakage flow, allowing high-pressure fluid to return to low-pressure regions and effectively providing a “bypass connectivity” during startup. This improved connectivity reduces ice-related risks in two ways. First, leakage flow introduces additional momentum and disturbance into near-wall low-velocity regions, weakening or disrupting stagnant structures. Second, the main flow channel becomes more continuous, recirculation zones shrink in scale, and ice crystals are more readily discharged along well-defined pathways, reducing their residence probability in sensitive regions. Consequently, moderate clearance enlargement is generally associated with improved passing stability and a lower tendency for localized ice accumulation.

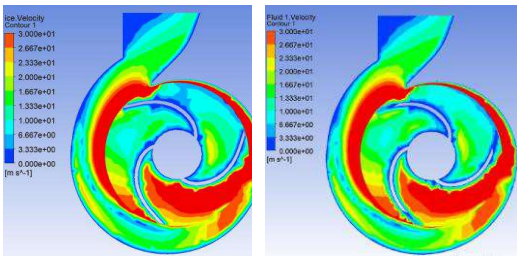
When the clearance is further increased, the internal flow becomes smoother, and closed recirculation and stagnant regions are further suppressed, providing ice crystals with more available discharge paths and reducing the likelihood of local blockage from a startup reliability perspective. However, excessive clearance may also exacerbate volumetric losses and compromise steady-state head and efficiency. Therefore, for ice-laden cold startup scenarios in polar environments, clearance design should prioritize startup reliability constraints while maintaining acceptable steady-state performance, with the optimal range determined through a combined consideration of driving margin and efficiency requirements.



（a）1800（t/10）

0.8

（b）1800（t/10）[1]



（c）1800（t/10）

1.5

（d）1800（t/10）[2]

Figure13 Seawater pump velocity cloud map

4. Conclusions

(1) Compared with pure seawater conditions, the cold-start process of seawater pumps under polar low-temperature ice-laden conditions exhibits markedly stronger unsteady characteristics. The presence of ice crystals alters the internal flow structure and energy transfer mechanisms, leading to increased shaft power demand, delayed establishment of steady head, and a pronounced tendency for local ice-crystal accumulation and retention. The results demonstrate that even at moderate volume fractions, the ice phase exerts a non-negligible influence on start-up load and reliability, and its multiphase effects must be explicitly accounted for in cold-start analyses..

(2) The start-up acceleration profile directly governs the rate of speed establishment and, consequently, the characteristic time scale, peak torque, and cumulative energy consumption during start-up. The results indicate that a smaller acceleration index can effectively shorten the start-up duration and reduce total start-up energy consumption, albeit at the cost of elevated transient peak torque. Conversely, a larger acceleration index mitigates transient mechanical loads but results in longer start-up times and higher energy expenditure. This highlights a clear trade-off among time efficiency, energy consumption, and peak load in variable-acceleration start-up strategies.

(3) The impeller–volute clearance reshapes the internal flow evolution by modifying leakage flow intensity and flow connectivity at the structural level. Numerical results show that a moderate increase in clearance weakens low-velocity stagnation zones and closed recirculation structures during start-up, accelerates the establishment of steady head, and effectively reduces peak torque and start-up energy consumption, while simultaneously alleviating the risk of short-term ice-crystal accumulation. However, further enlargement of the clearance introduces additional volumetric losses and may degrade steady-state efficiency, indicating that clearance optimization requires a careful balance between start-up reliability and steady performance.

(4) For polar ice-laden cold-start applications, the results suggest that priority should be given to improving flow connectivity and ice-crystal passability during start-up through structural parameter optimization, particularly clearance adjustment, as it provides a more direct and robust means of suppressing local accumulation and reducing blockage risk. On this basis, start-up acceleration strategies can then be refined to fine-tune start-up time, energy consumption, and peak torque, avoiding excessive transient mechanical loads induced by overly rapid acceleration. This

"structure-first, control-second" optimization sequence offers clear engineering guidance for the cold-start design of seawater pumps operating in polar environments.

Funding Declaration

This study did not receive any funding.

Conflict of Interest

The authors declare that there are no conflict of interests， we do not have any possible conflicts of interest.

Author Contribution Declaration

Conceptualization, Supervision, Project administration: Fukang Ma ;
Data curation, Formal analysis, Investigation, Methodology, Software, Validation, Writing–original draft: Yuxiang Chen;
Visualization: Chiyu Wang, Lingfei Kong, Zhengyang Liu, Kai Zhang, Ruifan Xu.

Data availability statement

All data generated or analysed during this study are included in this published article.

References

1. Schneck C C, Ghobrial T R, Loewen M R. Laboratory study of the properties of frazil ice particles and flocs in water of different salinities[J]. The Cryosphere, 2019, 13(10): 2751-2769.
2. Barrette P D. Understanding frazil ice: The contribution of laboratory studies[J]. Cold Regions Science and Technology, 2021, 189: 103334.
3. Chen Y, Lian J, Zhao X, et al. Advances in Frazil Ice Evolution Mechanisms and Numerical Modelling in Rivers and Channels in Cold Regions[J]. Water, 2023, 15(14): 2582.
4. Richard M, Morse B. Multiple frazil ice blockages at a water intake in the St. Lawrence River[J]. Cold Regions Science and Technology, 2008, 53(2): 131-149.
5. Daly S. Laboratory investigation of trash rack freezeup by frazil ice[J]. 1992.
6. Richard M, Cornett A. NRC frazil ice research facility[C]//Proceedings of the Annual Conference of the Canadian Society of Civil Engineering, Montreal, QC, Canada. 2019: 12-15.
7. Daly S F, Barrette P D. Prevention of water intake blockage by ice during supercooling events[J]. Journal of Cold Regions Engineering, 2023, 37(1): 03122001.
8. Chalghoum I, Elaoud S, Akrout M, et al. Transient behavior of a centrifugal pump during starting period[J]. Applied Acoustics, 2016, 109: 82-89.
9. Cheng L, Zhang K Y, Zhang Y L, et al. Effect on starting modes on centrifugal pump performance[J]. Processes, 2022, 10(11): 2362.
10. Perissinotto R M, Verde W M, Biazussi J L, et al. Flow visualization in centrifugal pumps: A review of methods and experimental studies[J]. Journal of Petroleum Science and Engineering, 2021, 203: 108582.
11. Kim B, Siddique M H, Bellary S A I, et al. Investigation of a centrifugal pump for energy loss due to clearance thickness while pumping different viscosity oils[J]. Results in Engineering, 2023, 18: 101038.
12. Ayad A F, Abdalla H M, Abou El-Azm A. Study of the effect of impeller side clearance on the centrifugal pump performance using CFD[C]//ASME International Mechanical Engineering Congress and Exposition. American Society of Mechanical Engineers, 2015, 57465: V07AT09A037.
13. Adistiya S, Wijayanta A T. Effect of clearance gap on hydraulic efficiency of centrifugal pump[C]//AIP Conference Proceedings. AIP Publishing LLC, 2019, 2097(1): 030053.
14. Chisely E A. Two-phase flow centrifugal pump performance[M]. Idaho State University, 1997.
15. Chen J, Chen X, Li W, et al. Research on two-phase flow and wear of inlet pipe induced by fluid prewhirl in a centrifugal pump[J]. Journal of Marine Science and Engineering, 2024, 12(6): 950.
16. Daly S. Laboratory investigation of trash rack freezeup by frazil ice[J]. 1992.
17. Safa N. Designing of frazil ice test rig[J]. 2015.
18. Barrette P D. A tabulated review of 83 laboratory studies on frazil ice[C]//IAHR International Symposium on Ice. 2020, 745.
19. Yang D, Lian J, Zhao X, et al. A mathematical model for supercooling process and its application to frazil ice evolution[J]. Scientific Reports, 2023, 13(1): 5801.
20. Amoresano A, Langella G, Niola V, et al. Advanced image analysis of two-phase flow inside a centrifugal pump[J]. Advances in Mechanical Engineering, 2014, 6: 958320.
21. Ghobrial T, Pierre A, Boyd S, et al. Ice accumulation at a water intake: a case study on the Mille-Iles River, Québec[J]. Canadian Journal of Civil Engineering, 2023, 51(2): 162-173.

Supplementary Files

This is a list of supplementary files associated with this preprint. Click to download.

- Articlehighlights.docx
- DeclarationofInterestStatement1.docx